Electron beam induced modification of nickel coated molybdenum surfaces

Y. Q. Yan*, J. Senkara and W. Włosiński
Warsaw University of Technology, Welding Department, 85 Narbutta Street, 02-524 Warsaw (Poland)

(Received March 19, 1991)

Abstract

The paper presents the results of research carried out to produce Ni–Mo layers by melting with an oscillating electron beam a 40 μm thick galvanic nickel layer deposited onto a molybdenum surface. The power density of the beam, treated as a rectangular-Gaussian surface heat source, has been regulated in the range of 10^9–10^{10} W m^{-2} and the exposure time was from 12.5 to 60 ms. The ranges for which continuous surface layers were obtained are presented. Within these ranges, the relations of thickness and structure of layers with the above-mentioned parameters are given. On the basis of structural testing (optical microscopy, scanning electron microscopy, electron probe microanalysis and X-ray diffraction) as well as microhardness measurements, the mechanism of formation of the layers is proposed.

1. Introduction

One of the fields for applying electron beams in materials engineering can be the modification of metal surfaces in such processes as cladding or alloying, *i.e.* processes of melting material layers spread onto surfaces of a different chemical composition. Special advantages of electron beam (EB) technology in this usage are: a high power density with little penetration depth into the material, easy and precise control, rapid heating and cooling of the surface layer and high energy efficiency of the process. In earlier work [1] the melting of powder mixtures on a tungsten surface by a scanned, defocused EB was presented in order to obtain Cu–Ti–Ta multi-phase surface layers. The method and device used in the present work are similar. However, due to other characteristics of the melted coating (a galvanic layer instead of powders), different conditions were applied: *i.e.* a focused EB oscillating in only one plane.

The method was used to obtain Ni–Mo coatings on a molybdenum surface. A modification of this kind seems interesting for joining molybdenum to ceramic materials and to metals creating neither solutions nor intermetallic compounds with molybdenum. It may also be effective because of the high corrosion resistance of Ni–Mo alloys in agressive environments.

*Permanent address: Beijing Polytechnic University, Department of Metallic Materials Science and Engineering, Beijing 10 00 22, China.

Figure 1 presents the Ni–Mo phase equilibrium diagram according to ref. 2. Its characteristic feature is the relatively wide range of α solid solution of molybdenum in nickel changeable with temperature and the low solubility of nickel in molybdenum (ϵ). In this system the phases β, γ and δ also occur on the basis of intermetallic compounds, Ni_4Mo, Ni_3Mo and NiMo respectively.

2. Experimental details

A 99.9% purity molybdenum sheet 1 mm thick was used as a substrate. The sheet was cut into 120×30 mm strips. The specimens were then cleaned, etched and galvanically covered with pure nickel. As a result, nickel layers with a matt surface and thickness of about 40 μm were obtained (Fig. 2). The characteristic texture

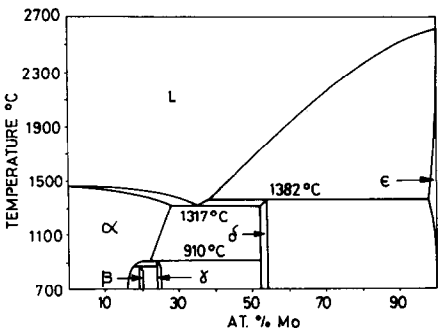

Fig. 1. Ni–Mo phase equilibrium diagram [2].

0257-8972/91/$3.50

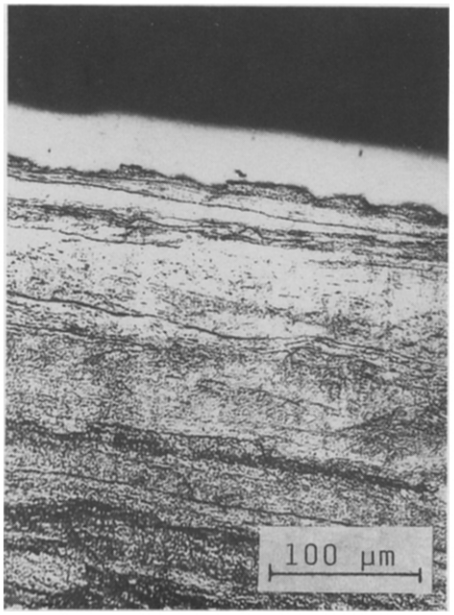

Fig. 2. Optical micrograph of molybdenum specimen galvanically coated with nickel.

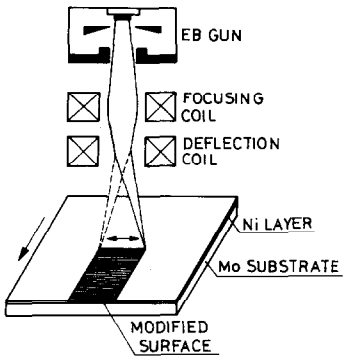

Fig. 3. Scheme of surface modification method used.

of the substrate with elongated grains, typical for material after rolling, can be noticed.

Specimens prepared in such a way were then treated with an electron beam. An electron beam welder of 6 kW power and 25 kV accelerating voltage, additionally equipped with a dynamic deflection system, was used. The specimens were moved under the oscillated EB, deflected in the plane perpendicular to the direction of movement with a frequency of 15.6 kHz. A path of melted material was produced on the surface. The oscillating EB was then the surface heat source, contrary to electron beam welding in which the conditions of so-called deep penetration are used. The scheme of the method is presented in Fig. 3. It was the band method applied with moving rectangular-Gaussian distribution of power on the surface as presented in Fig. 4. According to the classification of Arata [3, 4] it is one of the three kinds of surface heat sources. The distribution of power W on the specimen surface is

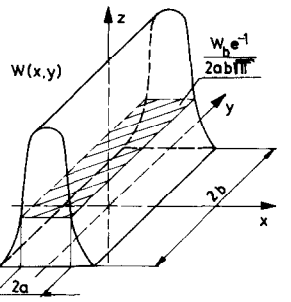

Fig. 4. Surface heat source with rectangular-Gaussian distribution of power [3, 4].

given by the formula

$$W = \frac{AW_b}{2ab\pi^{1/2}} \exp(-x^2/a^2)$$

where W_b is the EB power, A the surface absorption coefficient, and a and b are parameters of the heated material band.

The radius of the beam spot (the parameter a in Fig. 4) was 0.25 mm and the oscillation amplitude 10 mm ($2b$ parameter) was used in all the experiments. The vacuum level was 10^{-3} Pa and the exposure time was regulated by the speed of specimen movement in the range of 8–40 mm s^{-1}. The power of the EB was controlled by changing the beam current with constant acceleration voltage equal to 22.5 kV. This corresponded to an exposure time range of 12.5–60 ms and power density of 10^9–10^{10} W m^{-2}.

For structural tests of the specimen obtained, optical (OM) and scanning electron microscopy (SEM) as well as electron probe microanalysis (EPMA) were used. Phase analysis by the X-ray diffraction method (XRD) was also carried out. The microhardness (μHV) of the specimens was also tested.

3. Experimental results and discussion

3.1. Choice of parameters to produce layers

A distinct relationship was observed between the power density of a surface heat source and the exposure time on the one hand, and the appearance and structure of obtained layers on the molybdenum surface on the other. With low beam currents and high movement speeds the layers were not continuous. There remained local areas of unmelted nickel and the layer surface was very uneven. This was the effect of crystallization of single nickel drops insufficiently wetting the substrate due to its too low temperature. In turn, with high currents and low movement speeds the layer material evaporated and deep melting and cracking of the substrate could even be observed. However, there was a range of parameters for which continuous surface layers

were obtained. In Fig. 5 the above-mentioned results are shown in a coordinate system of exposure time (speed of movement) *vs.* EB power density (beam current). The area for which continuous surface layers had been obtained is shaded. The conditions under which the structure of samples was tested are also marked. The bold points correspond to the sample structures which are shown in Figs. 7, 8 and 9.

3.2. *Microscopic tests*

The structure tests were carried out by microscopic methods (OM and SEM) for 10 specimens according to different places in the area shaded in Fig. 5. The surface layers had single- or multi-phase composition in relation to the parameters of their formation process. The thickness of the layers as well as the depth of the recrystallized zone of the substrate varied. The latter rose monotonically with the increase of heat source power embracing in the end the whole cross-section of the substrate.

Figure 6 presents an example relationship between the average thickness of the surface layer and the beam current for the movement speed of 9.4 mm s^{-1}. The layer thickness decreases with increasing beam power, reaching its minimum and then beginning to increase up to a value exceeding more than twice the thickness of the initial nickel layer.

Figure 7(a, b) shows the microstructure of the specimen with minimum layer thickness in the cross-section perpendicular to its surface. It was obtained with a beam current of 50 mA and movement speed of 9.4 mm s^{-1}. The figure also presents the nickel distribution map and linear profile of molybdenum concentration.

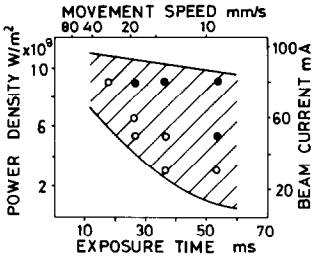

Fig. 5. The range of obtaining continuous Ni–Mo surface layers. The bold points correspond to specimens for structural testing.

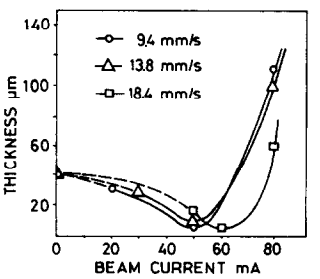

Fig. 6. Thickness of surface layer *vs.* beam current.

The thickness of the layer is about 5 μm, so a substantial part of the material must have evaporated. The layer has the single-phase structure of α Ni–Mo solution. The varying molybdenum concentration in the surface layer did not exceed 25 at.%. The substrate was not melted. Large regular molybdenum grains are visible after the recrystallization process.

In Fig. 8(a, b, c) the cross-sections through surface layers are presented for specimens obtained with the same high power density ($I_b = 80$ mA) and three different movement speeds: 18.4, 13.8 and 9.4 mm s^{-1}. These conditions correspond to successive points in Fig. 5. Figure 9(a, b, c) shows the surface nickel distribution in these specimens. All layers have a two-phase structure. Due to the action of the high power density heat source, the substrate becomes partially melted during the process. The samples are characterized by substantial structural modifications. The low nickel content phase occurs in the shape of dendrites on the background of the darker matrix. The quantity of dendrites increases with prolonged exposure time. The intermediate layers are formed at the surface layer–substrate interface. Quantitative EPMA results of the specimens shown in Figs. 7 and 8 are presented in Table 1.

The chemical composition of the dendrites and intermediate layers is similar. The nickel concentration in different places in the matrix fluctuated in the range of about 2 at.% while differences for the second phase were minimal. The results in Table 1 are the average values of three or four measurements.

The results of analysis show that dendrites are the most likely precipitates of the ϵ phase, in which the nickel content exceeds the maximum solubility of this element in molybdenum on the phase equilibrium diagram (1.5 at.% at 1370 °C). However, one must take into account the rapid crystallization of the Ni–Mo liquid solution from the temperature range above the melting point of molybdenum. The matrix – an alloy with a little more than 50 at.% molybdenum content – corresponds to the δ phase composition. However, cooling of the liquid layer on the molybdenum surface after relocation of the heat source departed considerably from the equilibrium conditions. For the above-mentioned reasons, a phase analysis was carried out in addition to the chemical composition analysis.

3.3. *X-ray phase analysis*

A Philips X-ray diffractometer was used for testing. Monochromatic Co Kα radiation was applied. The specimen from Figs. 8(b) and 9(b) was analyzed and the results are presented in Table 2. Only the lines with the biggest intensity are chosen. The results show that ϵ is the dominant phase in the layer (the ϵ phase and pure molybdenum have practically the same lattice

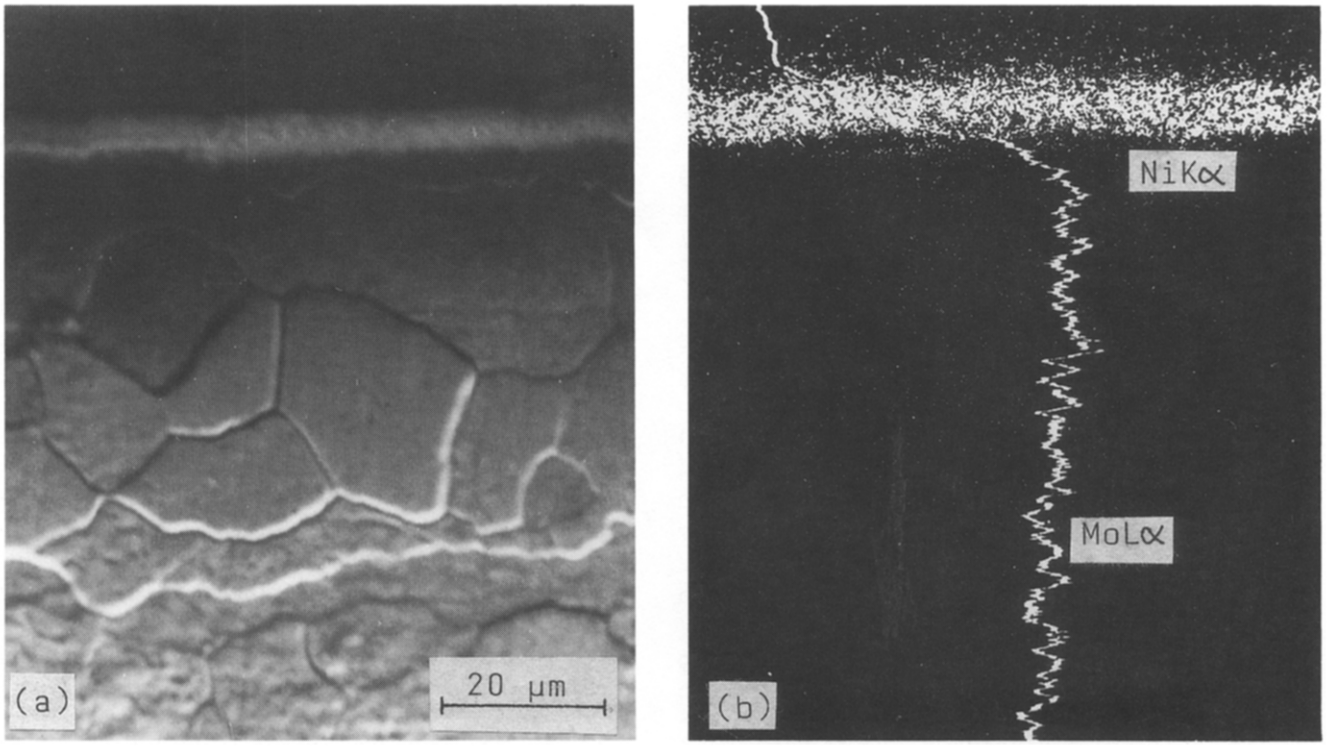

Fig. 7. Backscattered electron image (a), a map of nickel and linear molybdenum distribution (b) in the specimen obtained by $I_b = 50$ mA and $v = 9.4$ mm s^{-1}.

parameters, in the range of error). Substantial quantities of α and δ phases are also detected.

Based on the results of microscopy, EPMA and XRD it can be stated that the matrix of the layer is the α solution. The second ϵ phase is distributed inside it in the form of numerous dendrites. The lattice parameter of the α phase was calculated as 0.362 nm, which corresponds to the maximum molybdenum concentration in the nickel lattice. This remains in good agreement with results calculated from the extrapolated empirical formulas for the Ni–Mo solution published by Brooks *et al.* [5] and Kayser [6].

In the matrix of the layer, the δ phase also exists, most probably in the form of small inclusions, noticeable near the boundary with the ϵ phase under high magnification (Fig. 9(b)). The chemical composition of the layer matrix previously measured by electron microprobe (Table 1) is thus an average composition of α base and also δ and ϵ phases with large dispersions.

The lines characteristic of the γ phase have not been found. This phase is formed as a result of a peritectoidal reaction, the course of which is not possible during rapid cooling.

However, the existence of the β phase, which is the superlattice of α phase, becomes an open question. There are lines on the diffraction pattern which could result from that phase. The line broadening observed may result, however, from the existence of dual or triple β lines or from the variable lattice parameter of the α solution, connected with a probable concentration gradient of molybdenum. The schematic diffraction patterns of both α and β phases according to ref. 6, illustrating the above-mentioned statement, are shown in Fig. 10(a, b).

Barskaya *et al.* [7] have detected the δ phase at grain boundaries and inside the grains in Ni–22 at.% Mo alloys after quenching in water. However, the lines from the β and γ phases appeared only after tempering at 800 °C. The results confirm the conclusion that the probability of forming both of these phases under rapid cooling conditions is low.

3.4. Microhardness testing

The results of microhardness testing should be treated in our case as supplementary. A Neophot 2 optical microscope equipped with a Hannemann objective has been used. A load of 0.98 N was applied.

The microhardness of the initial galvanic coating of nickel was μHV 0.1 = 91.5. For a single-phase surface layer the measurement was not possible due to its small thickness (about 5 μm). For multi-phase layers the results obtained should be treated as average values for phases with different microhardness. The results of the tests are presented in Fig. 11(a, b) as a function of the movement speed and beam current. Every point is the average of 15 measurements.

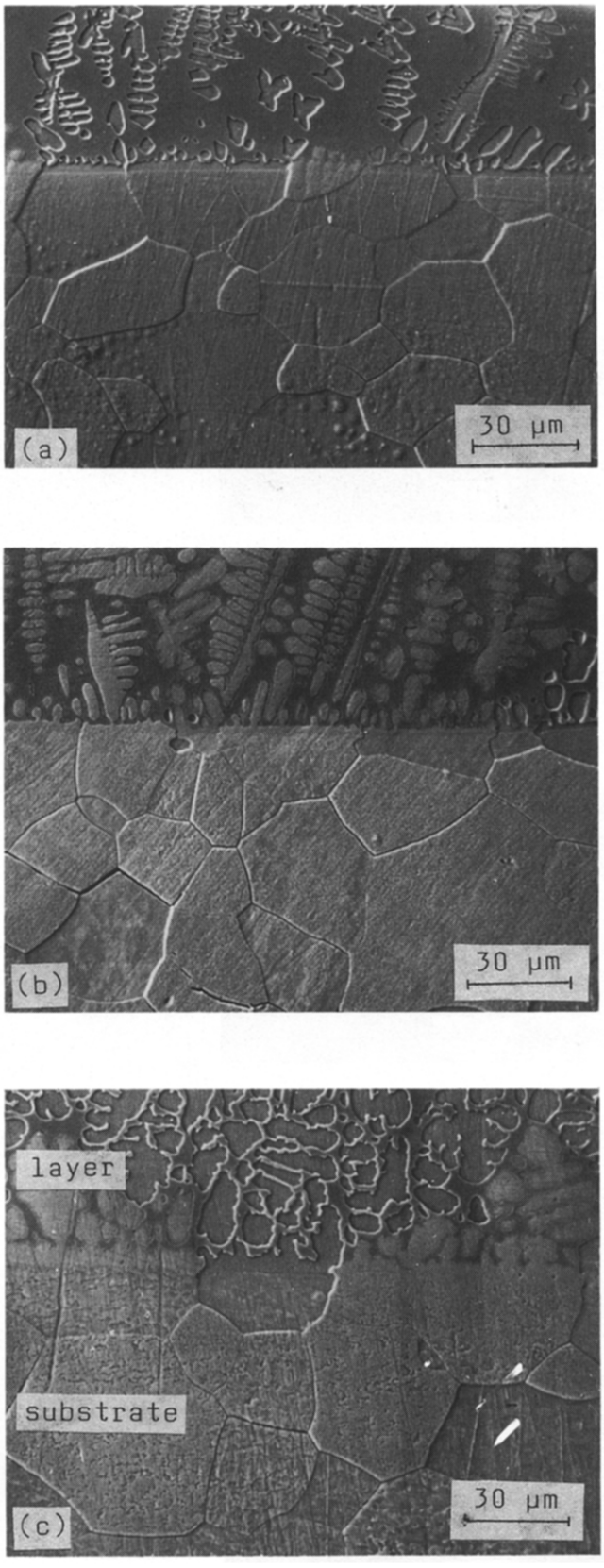

Fig. 8. Secondary electron images of specimens obtained with beam current of 80 mA and various speeds of movement: (a) 18.4; (b) 13.8; (c) 9.4 mm s^{-1}.

It is clearly visible that the microhardness of the layers rises with the increase of heat quantity delivered to the specimen (increase of beam current or decrease in movement speed). It is connected to the increasing content of the ϵ phase. The thickness of the Ni–Mo layer, which is characterized by a considerably higher hardness than recrystallized molybdenum, rises in a similar way. The μHV graphs correlate with the results presented in Fig. 6.

4. Conclusions: mechanism of layers forming

On the basis of the tests carried out it can be concluded that the power density and exposure time are of prime importance in obtaining good Ni–Mo surface layers. The parameters mentioned decide the structure of the continuous layer obtained. Two cases can be distinguished:

(1) the power density of the EB is not sufficient to melt the substrate;

(2) molybdenum is partially melted.

In the first case the galvanic nickel layer on the molybdenum surface is melted under the influence of the delivered heat. With a sufficiently high power density for the heat source and long exposure time the substrate becomes heated and wetted by liquid nickel. Molybdenum begins to dissolve intensively in liquid nickel. The concentration profile of this element in the layer testifies to this. The α solution layer forms on the substrate, according to the phase equilibrium diagram. The diffusion of nickel into the substrate is not observed due to the poor solubility of this metal in molybdenum and the short time of mutual interaction at high temperature.

The thin surface layer of molybdenum passes into the liquid state as a result of the high power density of the EB. A liquid Ni–Mo solution is then formed by mixing of the two liquids. After movement of the heat source, rapid crystallization occurs: the ϵ phase appears and at the substrate–liquid interface a clear intermediate layer of similar composition is formed. With the further decrease of temperature the α and δ phases crystallize.

The final thickness of the layers obtained is a result of intense evaporation of nickel from the liquid phase in vacuum on the one hand and a partial melting of the substrate on the other. The characteristic shape of the curve in Fig. 6 can be explained by these facts. With the increase of power density the temperature of liquid nickel rises and so does the evaporation rate. The layer thickness reaches a minimum. After partial melting of the substrate and creation of a liquid solution the evaporation rate decreases and simultaneously increases the volume of liquid.

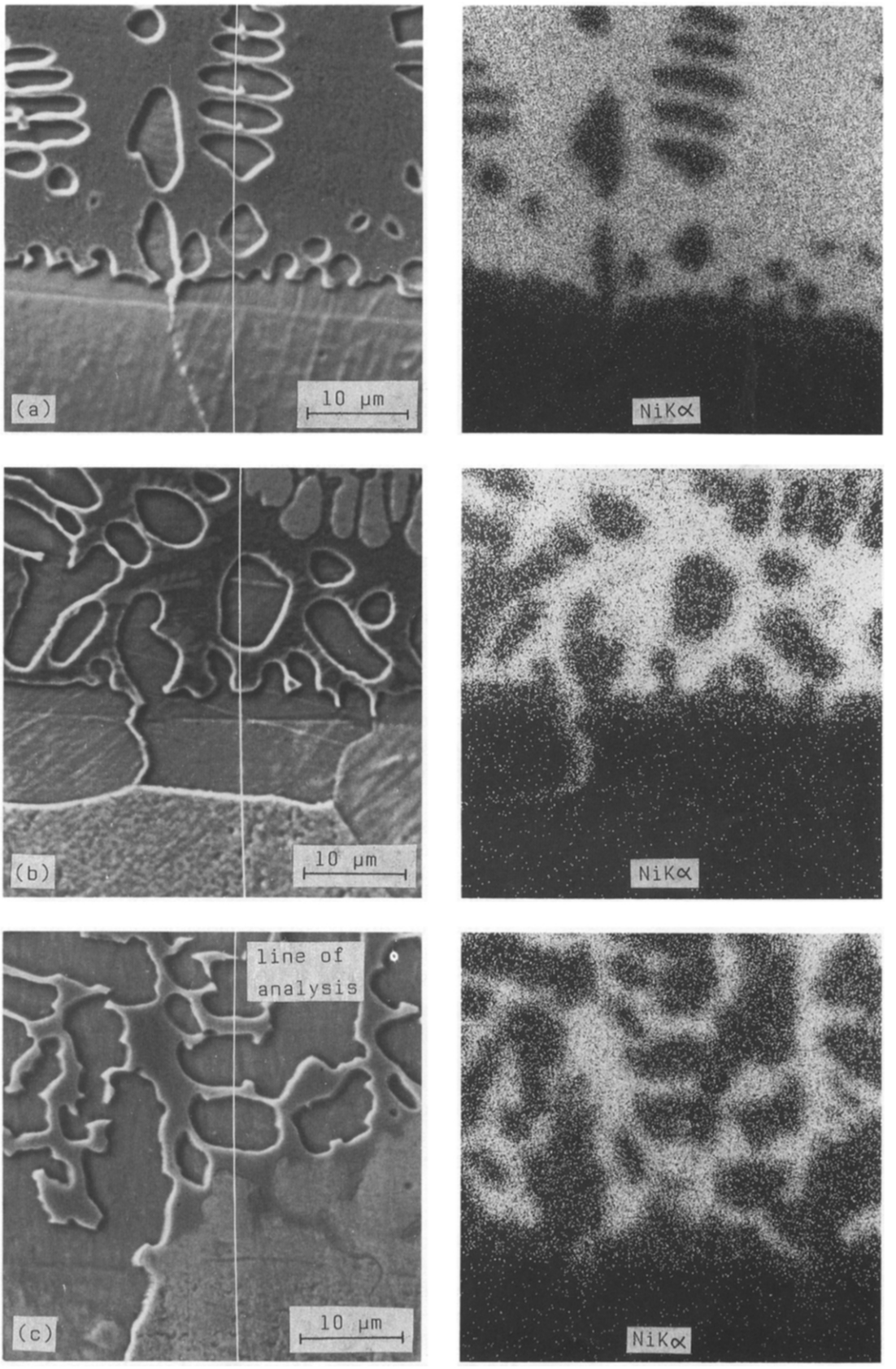

Fig. 9. Maps of nickel distribution in samples from Fig. 8 (the same designations).

TABLE 1. Quantitative EPMA results of Ni–Mo surface layers (average values)

Specimen from Fig. No.	Matrix		Second phase	
	at.% Ni	at.% Mo	at.% Ni	at.% Mo
7	Balance	25 <[a]	–	–
8(a)	45.4	Balance	3.4	Balance
8(b)	47.7	Balance	3.3	Balance
8(c)	48.5	Balance	3.2	Balance

[a]Variable molybdenum concentration in the range of 0–25 at.% in the direction from the surface to the substrate.

TABLE 2. Specification of high intensity diffraction lines for specimen presented in Fig. 8(b)

No. of line	2θ	Line	dθ	Intensity	Phase identified
17	43.45	Kα	2.418	1	δ
19	47.29	Kα	2.232	100	ϵ (Mo)
20	47.37	Kα	2.228	60	ϵ (Mo)
21	47.95	Kα	2.203	6	δ
24	50.70	Kα	2.091	13	α
26	51.65	Kα	2.055	2	δ
27	52.17	Kα	2.036	3	δ
28	53.35	Kα	1.994	1	β(?)
32	59.50	Kα	1.804	2	α
35	69.17	Kα1	1.576	70	ϵ (Mo)
38	88.26	Kα2	1.287	11	α
44	110.50	Kα2	1.089	1	α
46	117.85	Kα2	1.045	1	α
48	127.91	Kα1	0.996	35	ϵ (Mo)

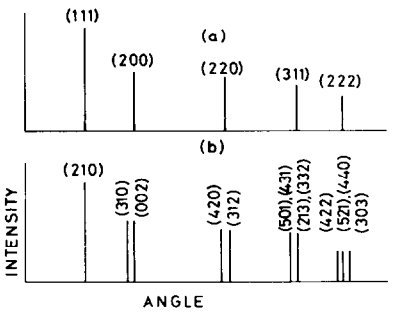

Fig. 10. Schematic diffraction pattern of α (a) and β (b) phases in the Ni–Mo system [6].

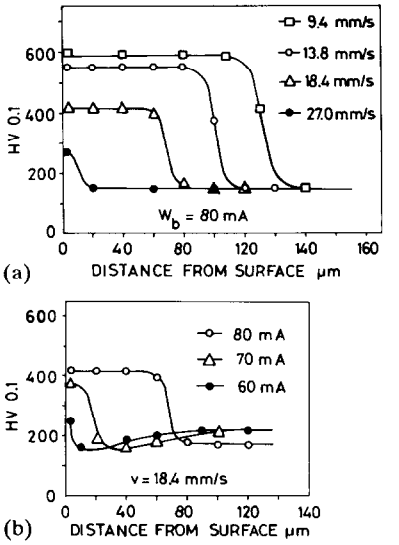

Fig. 11. Microhardness of specimens as a function of movement speed of a heat source (a) and beam current (b).

The thickness of the recrystallization zone in the substrate rises monotonically with the increase of beam power density and exposure time: it is proportional to the amount of heat delivered.

Acknowledgments

The work was sponsored by CPBR 2.4. The authors thank Dr. M. Psoda for XRD tests and helpful discussion. The preparation of metallographical specimens by Eng. J. Jakubowski is also greatly acknowledged.

References

1 J. Senkara, *J. Mater. Sci. Lett.*, in press.
2 T. B. Massalski (ed.), *Binary Alloy Phase Diagrams*, Am. Soc. of Metals, Metals Park, OH, 1986, p. 1611.
3 Y. Arata, *Plasma, Electron and Laser Beam Technology*, Am. Soc. of Metals, Metals Park, OH, 1986, p. 15.
4 Y. Arata, *Development of ultra high density heat source and its application to heat processing*, Japan Soc. for the Promotion of Welding, 1985; Polish translation, Wrocław, 1986, p. 23.
5 C. R. Brooks, J. E. Spruiell and E. E. Stansbury, *Int. Met. Rev., 29* (1984) 210.
6 G. F. Kayser, *J. Mater. Sci., 24* (1989) 2677.
7 R. A. Barskaya, J. B. Sidorova and Z. J. Dzeladze, *Poroskhovaya Metalurgia, No. 11* (1989) 82.